Potential application of CeO_2/Au nanoparticles as contrast agents in optical coherence tomography

H. ULLAH[1,*], Z. BATOOL[1], A. NAZIR[1], K. AHMED[1], M. RASHEED[1], FATIMAH S. AL-KHATTAF[2], G. GILANIE[3], MUHAMMAD UMAR DAD[4], S. HABIB[5]
[1]*Biophotonic Imaging Techniques Laboratory, Institute of Physics, The Islamia University, Bahawalpur, Pakistan*
[2]*Department of Botany and Microbiology, College of Science, King Saud University, P.O. Box 2455, Riyadh 11451, Saudi Arabia*
[3]*Department of Artificial Intelligence, Faculty of Computing, The Islamia University of Bahawalpur, 63100, Pakistan*
[4]*School of Physics and Electronic Science, East China Normal University, Shanghai 200062, China*
[5]*Institute of Chemistry, The Islamia University, Bahawalpur, Pakistan*

The current work explores the potential application of CeO_2/Au core shell (particle size ranging between 30-40 nm) that were competently synthesized and were confirmed through characterization technique of XRD, diffuse reflectance spectroscopy, and UV-VIS spectroscopy in emerging imaging modality optical coherence tomography (OCT) as contrast agent. These nanoparticles were also successfully analyzed in water and blood plasma phantom to measure their scattering coefficients and relaxation times under dynamic light scattering in Brownian motion. The K-edge values were calculated using CeO_2 NPs as core effect that have application in OCT. The Au has been observed to be a good contrast agent in OCT and have higher scattering coefficient that CeO_2. The particles were formed using unique pot green function and Z, keeping PH at 7. Starch was added to target the tumour. Therefore, the current work assures that Cerium and Gold Core-Shell nanoparticles have significant applications in the improvement of OCT imaging.

(Received March 14, 2022; accepted July 30, 2024)

Keywords: CeO_2/Au, Contrast agents, XRD, Diffuse reflectance spectroscopy, UV-VIS spectroscopy, Optical coherence tomography

1. Introduction

1.1 (CeO_2 NPs) cerium oxide

From uncommon earth metal oxides, one of the most significant uncommon earth oxide is cerium oxide nanoparticles. It is utilized as a consuming impetus. The ability of Ce is to rejoin with the property of variable itself, oxygen breaks down and also reduction satiate, i.e., Ce4+ and Ce3+ makes it appropriate in the direction of synergistic reason. The reversible compound response is demonstrated as follows;

$$CeO2 = CeO2 - x + (x/2)\ O_2\ (x = 0 \text{ or } 0.5) \quad (1)$$

CeO_2 nanoparticles are highly effective catalyst due to their large surface area. This effect also makes them excellent oxygen buffering agent. A cerium oxide/zirconium oxide (CeO_2-ZrO_2) structure can be utilized to enhance thermal stability. This system also provides the improvement in the efficiency of CeO_2 for catalytic purpose. Diesel fuel combustion catalyst is another important application of CeO_2 which can reduce the fuel consumption. It also prevents the emission of harmful exhausts such as CO. The exhaust form of diesel fuel is a combination of highly toxic gases along with vapors and different kind of fine particulates. These diesel exhaust gases have air pollutants like carbon monoxide, different oxides of nitrogen, and volatile hydrocarbons. As a catalyst, Cerium oxide nanoparticles are used to convert these nitrogen oxides, CO and hydrocarbons into innocuous nitrogen, carbon dioxide and water. Through this auto exhaust treatment, oxygen is provided by CeO_2 nanoparticles which behave as an oxygen buffer agent. In Europe, CeO_2-based diesel fuel catalysts are commercially available.

Another major potential application of CeO_2 nanoparticle is the elimination of organics from wastewater as CeO_2 nanoparticles have the ability to provide its oxygen for the elimination of carbon monoxide and hydrocarbon [1].

1.2. Gold nanoparticles (Au)

Nature of gold nanoparticles is very different from macroscopic gold material. Gold nanoparticles appear as red colloidal solution as compared to its counterpart. Gold has reputation of being an inert metal but gold nanoparticles having diameter less than 5 nm becomes reactive. This property can be utilized in catalytical activity for many chemical reactions. Gold nanoparticles are very good at mild or ambient conditions. If it is used in combination with other nanoparticles like titanium oxide, it will show catalyst effect for CO gas as well. Their catalytic function changes with change in size as small particles have larger catalytic ability.

It is quite useful in the field of imaging. As gold nanoparticles have larger atomic number, so its attenuation

for x-ray is quite higher. That is why; it can be used as a contrast agent in x-ray tomography. Similarly, it can be used as contrast agent for all other techniques that operates with x-ray or gamma rays. It is a multifunction therapeutic agent as well. It is used to carry drugs to tumour's site with the help of targeting agent. This is the major benefit of Gold nanoparticles [2, 3].

Some investigation provides the fact that dendrimer entrap stabilized gold nanoparticles adapted with few acid groups similar to diatrizoic acid as well as folic acid includes greater x-ray attenuation and nanotoxicity [4-6]. Few novel gold nanoparticles have been used as distinguished particles for computed tomography scan investigated by Liu Y. *et al.* [7]. All aforementioned work explores the promising characteristics of various nanoparticles to be applied to increase the imaging capability of OCT[8, 9]. In this work; we have successfully implemented these particles for 2D structured OCT mapping in water and blood plasma phantom and to measure the optical parameters of these particles in these phantoms.

2. Materials and methodology

The following materials and chemicals were purchase from sigma Aldrich.

i) [($HAuCl_4 \cdot 3H_2O$)] Gold chloride tri-hydrate

ii) [(($Ce(NO_3)_3.6H_2O$)] Cerium nitrate hexa-hydrate

iii) [HOC (COONa) ($CH_2COONa)_2 \cdot 2H_2O$] sodium citrate de-hydrate

iv) (Thio-glycolic acid)

v) Distilled water

vi) Zingiberofficinale (ginger)

vii) Starch

2.1. Preparation of plant extract

Gold nanoparticles were synthesized by one pot green method. Firstly, plant's extraction was washed many times in distill water to get rid of impurity. For 7 hours, 20 g of plant extract was heated in 250 ml of distill water at boiling temperature with gentle stirring. Insoluble portions were removed using filtration method and stored in refrigerator at low temperature [10].

2.2. Preparation of gold nanoparticles

In 100 ml of distilled water, 1mM solution of gold chloride $HAuCl4.3H_20$ was made. The solution was heated until it started boiling and fumes were seen. After this 50 ml of plant extracted in the solution of gold, salt was added. It acts the same as capping and reducing agent as well with stable vigorous heating and exciting for 14 minutes. After that, 100 ml of solution was added with 75.5 mM sodium citrate, that is utilized to keep pH of solution and improve the reduction reaction with steady heating and vigorous stirring until the color of solution become red [11].

Cerium nanoparticles were also synthesized by one pot green method. In first step, the plant extraction was washed many times in distilled water to get rid of the impurity. For 7 hours, about 20 g of plant extraction in 250 ml of distilled water were heated at boiling temperature with steady stirring. Non-soluble portion were removed using filtration method and stored in refrigerator at low temperature. After that, 495 ml solution of 9 mM Cerium nitrate hexa-hydrate "[(($Ce(NO_3)_3.6H_2O$)]" was produced and heated at temperature of boiling through energetic stirring until it was started boiling. The solution of cerium salt i.e. 25 ml was added with zingiber officinale that worked as capping agent and reducing agent through steady strong stirring and heated for 14 minutes. After that, 55 ml solution was added with 766 mM 'sodium citrate', which is utilized to keep pH of solution. A strong stirring is continued until the color of solution becomes yellow. Solution was kept at room temperature to decrease the temperature [12].

In 1000 ml of solution prepared with same method as mentioned in the above section, 1mM gold salt was added and started heating at boiling temperature with slight heating. In this solution, Ce nanoparticles solution was added [13]. This solution was heated with gentle mixing until it becomes dark green and kept in room to get room temperature of the solution.

2.3. Addition of linker

These three nanoparticles are linked with thioglycolic acid. For this, 100 ml solution of aforementioned three different nanoparticles were prepared. These three solutions were added with 2% wt thioglycolic acid without heating at stable stirring for whole night. Physical appearance of these 3 solutions changed at next morning [14]. Au nanoparticle's solution became black, Ce became white and cerium and gold core shell structure became dark grey. After addition of targeting agent, non-visible nanoparticles became visible and nanoparticles were separated using centrifuge.

2.4. Adding targeting agent

Starch was used as targeting agent (TGA) for these nanoparticles. For this, in distilled water 100 ml of 1 wt % starch solution prepared thrice for described nanoparticles [15]. After it, 0.5 g of single nanoparticle was mixed in the starch solution and kept stirring without heating for whole night. Concluding solutions could be used as the targeted (CT) contrast agents.

3. Results

3.1. X-ray diffraction

The X ray diffraction is one of the mainly reliable and advance techniques that utilizes the lower wavelength of X rays[16]. The size of crystal (particle) is measured with the help of Sharer's equation. This method in addition is used

to measure structure and crystallinity of crystals. The Sharer's equation is given by;

$$\text{Crystallite size} = K\lambda/B\ \text{Cos}\theta \quad (2)$$

Here k = constant (value is 1), β = FWHM Value, (full width half maxima value) and θ = (incident angle) lies between incident beam of x ray and planes of crystallite. The XRD spectrum of cerium oxide, gold nanoparticles, and ceria-Gold nanoparticles is given in figure 1 (a-c).

The XRD spectrum of CeO_2 nanoparticles (Fig. 1(a)) gives the most intensity peak at 29.5, 34.5 and 48.5 value of "2θ" that correspond to the (111), (200) and (220) planes of crystallite structure of Cerium oxide. All these peaks correspond with available literature [17]. These outcomes confirm the arrangement of Ce NPs. The crystallite range of ceria NPs be approximately 29.04 nm, measured with the assistance of Sharer's formula[17].

Fig. 1(b) shows the XRD pattern of Au nanoparticles. Gold NPs show the highest intensity peaks at 39, 45, 65 and 79 rates of "2θ" illustrating the (111), (200), (220) and (311) plane of gold crystals shows cubic structure. The mean size measured with the use of Sharer's formula is 39.95 nm [18, 19].

Fig. 1(c) depicts the XRD pattern of cerium and gold core shell structure. The maximum intensity peaks of cerium and gold core shell which are 29, 35, 37, 44 and 47 are explaining the plane of Ce NPs (111), (200) and (220) respectively, here at 37 and 44 are the plane of Au shell which are (111) and (200). The mean size is approximately 37 nm [20]. Table 1 shows the intensity peak, FWHM and Particle size of gold, Cerium oxide and core shell CeO_2 @Au NPs.

Table 1. The intensity peak, FWHM and particle size of gold, Cerium oxide and core shell CeO_2 @Au NPs.

Materials	Peaks	FWHM	Particle's size (nm)
Cerium oxide	29.7955	0.4029	29.04
Gold	39.4021	0.2459	39.95
Core shell CeO_2@Au	32.5561	0.2459	37.02

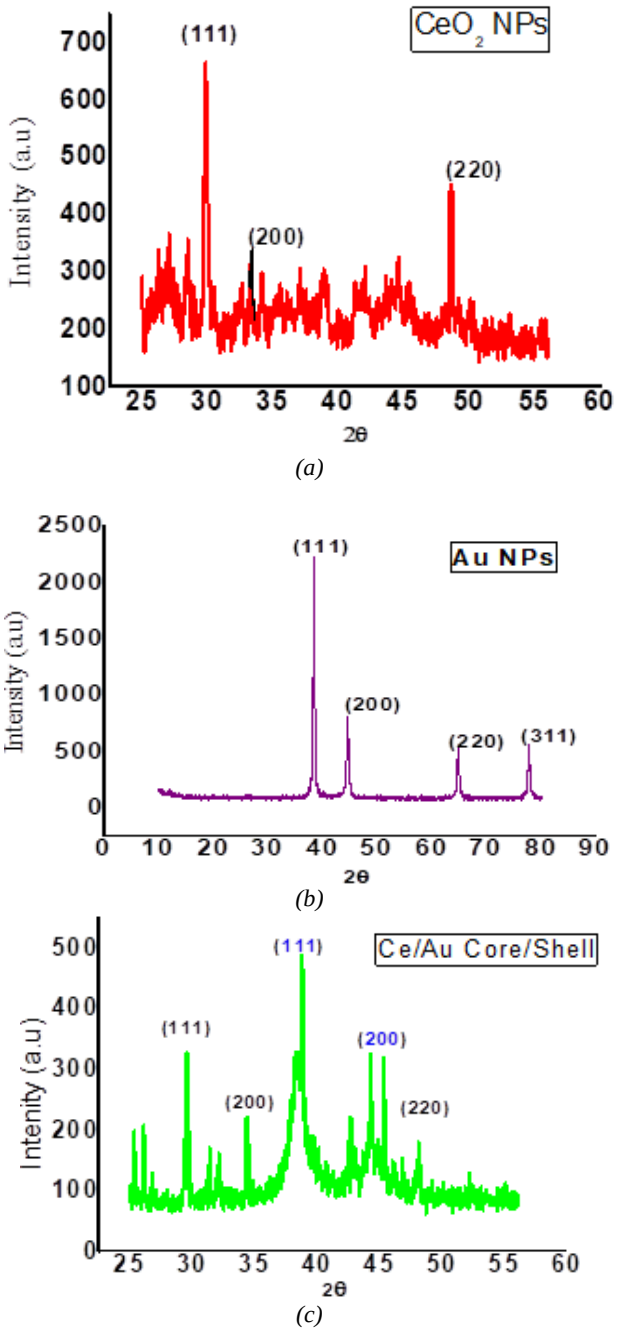

Fig. 1. XRD of (a) Cerium oxide nanoparticles, (b) Gold nanoparticles, and (c) Ceria-Gold nanoparticles (color online)

3.2. UV/VIS spectroscopy results

UV/VIS spectroscopic method has been used en route for understanding of the surface resonance, the absorption spectrum and SPR peaks of nanoparticles. UV/VIS Cecil 8000 machine [21] was used to get the UV/VIS spectrum of these nanoparticles. The spectroscopy was taken out at room temperature in ultra violet (200-400 nm) and visible region (400-800 nm). The results are described graphically in Fig. 2 (a). The peak of cerium nanoparticles has been observed at 282 nm in absorption spectrum. Ceria nanoparticles show maximum absorbance between the 275

nm - 325 nm. Our results are in good agreement with literature [22].

UV-VIS absorption spectrum of Au nanoparticles shows the peak absorbance at 524 nm as shown in figure 2(b). According to literature the spherical gold nanoparticles SPR peaks lies between in 500 nm – 550 nm. Therefore, our results are in concord with literature [23].

Spectrum of Cerium and gold core shell nanoparticles show that the absorbance peak appears at 285 nm (figure 2(c)). Simple ceria nanoparticles have slightly greater absorbance peaks than Cerium and gold core shell nanoparticles. This occurs because gold behaves as the shell and SPR peak lies at 524 nm of gold. Therefore, the peak of Ce-Au core shell nanoparticles has a little shift in the direction of the lower value as compare to simple CeO_2 nanoparticles. Thus, this consequence illustrates the production of structure having cerium and gold core shell. Table 2 shows the absorption peaks of gold, cerium and Cerium/gold core-shell along with the measured absorption values.

Table 2. The absorption peaks of gold, cerium and Cerium/gold core-shell

Material	Wavelength (nm)	Abs (a.u)
Au	524	0 .433
CeO_2	282	1 .730
Ce @ Au core shell	285	0 .425

3.3. Diffuse reflectance spectroscopy (DRS) techniques

DRS [24]techniques investigate optical behaviours of the nanoparticles; the DRS were also carried out in this work. NIR spectrometer lambda model 950 was utilized to carry out the measurements for DRS. The equipment offers the range of wavelengths 200-3300 nm but in our experiment, we have measured the DRS from 200 to 1300 nm to investigate all 3 nanoparticles i.e. CeO_2, Au and CeO_2@Au core shell. These outcomes of the spectrum are shown in Fig. 3 (a-c).

The spectrum of Ce nanoparticles illustrates that the absorbance of CeO_2 Nano particles lies between 206 - 373 nm. On the other hand, absorbance values of Au nano particles range from 253 nm - 610 nm. The core-shell of cerium and gold show greater absorbance is 275 nm – 580 nm that is lying between the CeO_2 and Au nanoparticles.

3.3. Study of energy bad gap

By using the percentage or diffuse reflectance spectrum, the energy band gaps of nanoparticles can be measured very easily. For this reason, the Kubelka Munk formula can be utilized as[25];

$$F(R) = [F(R\infty)\, hv]^2 \qquad (3)$$

F(R) = (Kubelka Munk Function)
R = represent the reflectance of absolute value (which is obtain by the assist of DRS procedure).

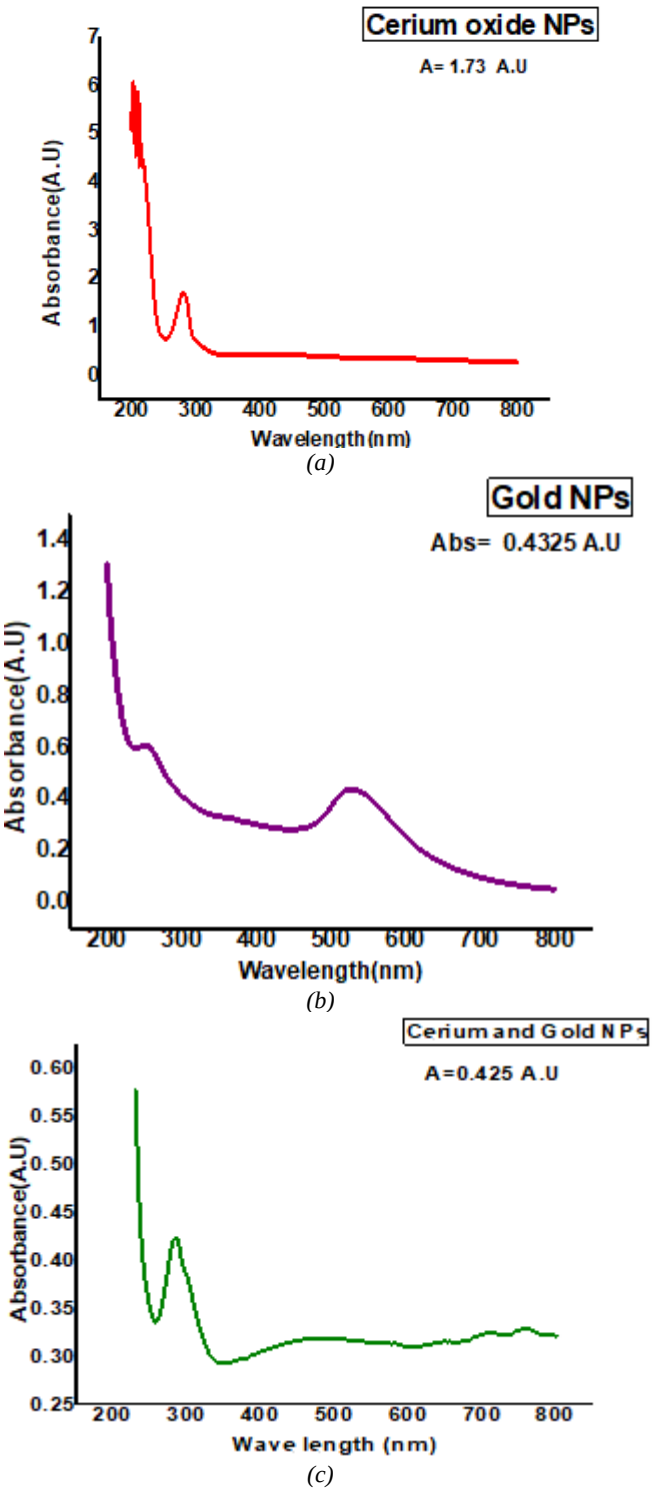

Fig. 2. UV/VIS Spectrum of (a) Ce nanoparticles, (b) gold nanoparticles, and (c) Cerium and Gold core shell nanoparticles (color online)

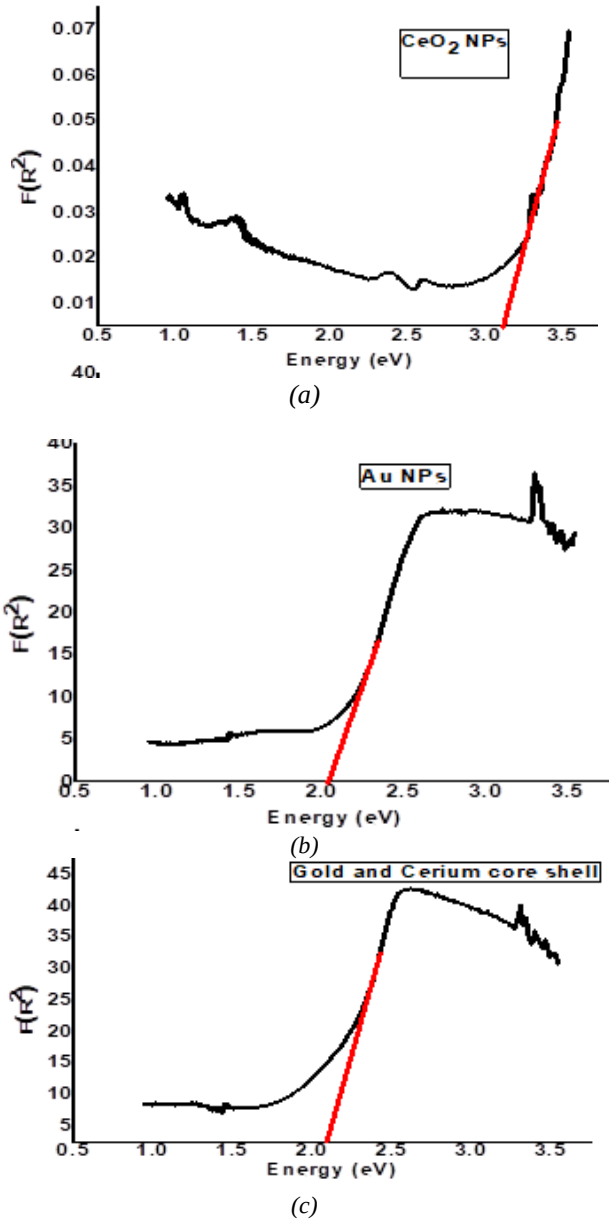

Fig. 3. Reflectance of (a) ceria nanoparticles against wavelength, (b) gold nanoparticles against wavelength, and (c) of core shell ceria-gold nanoparticles against wavelength (color online)

In the Fig. 4 (a-c), the energy band gaps of the nanoparticles are measured. The relationship is carried out between energy and F (R^2). Both variables have been computed by Kubelka Munk method. While on the y-axis of the figures we have F (R^2) and on the x-axis we have energy (eV). The energy band gap is measured through sketching tangent at the curve and intersection position on energy axis is the energy band gap value. Energy band gaps for gold, Ce and Ce-Au core shell are measured from the graph are given in the tabular form (Table 3)

The measured energy band gap for ceria NPs is 3.12 eV that matches with earlier findings in the literature that have the range of 3 - 3.2 eV for ceria NPs [26]. Similarly, for the gold NPs, our finding (our measured band gap 2.03 eV) is in good agreement with literature i.e., 2 eV - 2.4 eV.

For the cerium and gold core shell nanoparticles, the measured energy band gap measured 2.10 eV, which is slightly greater than (Au) gold and it also lesser than cerium oxide CeO_2 NPs may be due the surface properties that are dominant due to shell.

Table 3. Shows the energy band gaps of gold, Cerium oxide and gold and cerium core shell nanoparticles

Material	Energy B.G (eV)
CeO_2	3.12
Core shell of cerium and gold	2.10
Au	2.03

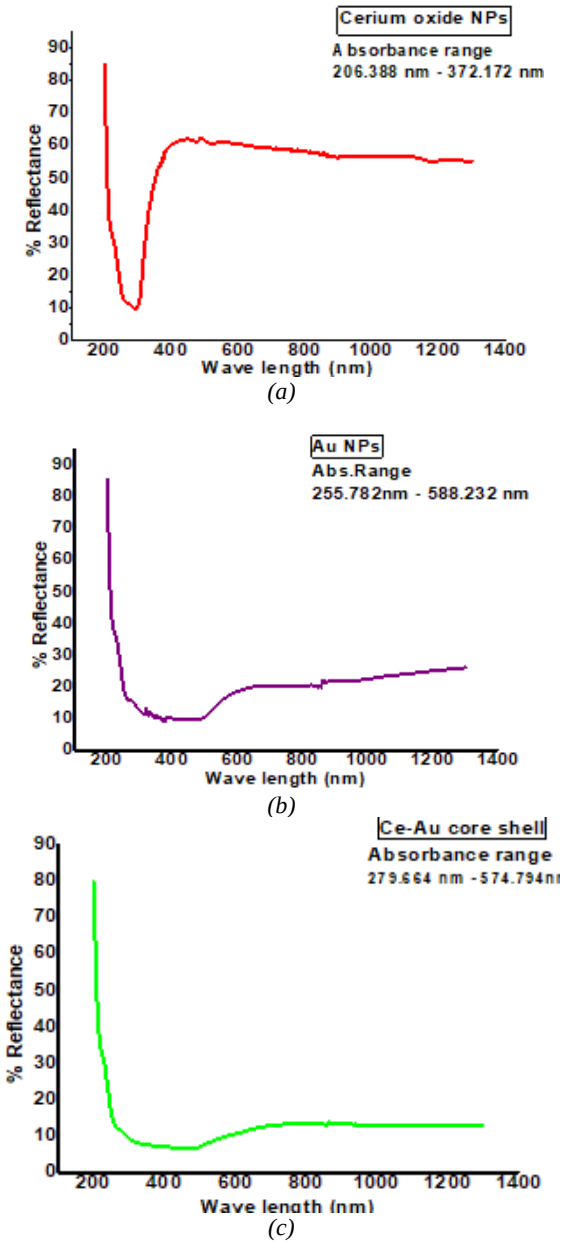

Fig. 4. (a) Band gap of ceria nanoparticles, (b) energy band gap of gold nanoparticles, and (c) band gap of ceria-gold nanoparticles (color online)

Our results of all three types of particles verify the production of nanoparticles. Firstly, consequences of UV/VIS spectroscopy show the absorbance peaks in conformity of literature data used for Ceria, Gold. The SPR peaks for Ceria NPs was at 282 nm while intended for gold NPs was at 524 nm as well as for the core shell structure it was 285 nm i.e., a little greater than for the Ceria core as the shell layer of "Au" have greater rate of wavelength of SPR Peak. As a result, this illustrates the formation of core-shell structure.

The visual behavior like absorbance of particle is in agreement with earlier reported values of these nanoparticles. In calculation toward this the energy band gaps, the energy band gaps of CeO_2 nanoparticles were 3.12 eV, for gold is lying on 2.03 eV and for CeO_2-Au core have the energy band gap of 2.10 eV. The range of absorbance values was in-between for core shell composition when compared with the gold and ceria nanoparticles.

4. Application in optical coherence tomography

Optical coherence tomography (OCT) is particularly promising. Using the principles of optical interferometry and coherence gating, OCT can yield micron-scale resolution subsurface images of tissues, with high sensitivity to details of biological structures/analytes that influence its measured backscattering signal [27-29]. The technique is attractive for real time *in situ* imaging approaching the limits of conventional histology (but without the need for tissue excision!), with penetration depth of 1~3 mm in most tissues, and with access to many body sites enabled by fibre optics implementation [30]. OCT's limitations include strong scattering of probing light from the biological tissues at the visible and near infrared (NIR) wavelengths, yet this is spectral range available for biophotonic diagnosis as dictated by the constraints of tissue optics.

We have used CeO_2 and Au nanoparticles to investigate the possible effect on dynamic light scattering underlying the Brownian motion in water, plasma and stagnant whole blood by exploring the autocorrelation function in M-mode scanning.

4.1. Scattering behaviour

4.1.1. Samples for OCT applications

Three types of scattering samples with varying nanoparticles concentrations were used in this investigation:

(I) Phantom with CeO_2

i) The first part of this set was water phantoms with 29.04 nm diameter CeO_2 with its six different concentrations 0.1, 0.12, 0.14, 0.16, 0.18, 2.0 (weight/volume i.e. spheres/micron^3). The refractive index of CeO_2 ~2.33 [31], and then μ_s was calculated from Mie theory at 1310 nm [32, 33]. The refractive index of water used was 1.33. The measured decorrelation times of CeO_2 and scattering coefficients are given in table 4.

ii) The second part of this set was blood plasma instead of water with 29.04 nm diameter CeO_2 with its six different concentrations 0.1, 0.12, 0.14, 0.16, 0.18, 2.0 (weight/volume i.e. spheres/micron^3). Whole blood was drawn from five months old female Fisher rats into heparin tubes that were then centrifuged to separate out the plasma. The refractive index of CeO_2 ~2.33 [31], and then μ_s was calculated from Mie theory at 1310 nm given in table 4 [32, 33]. Refractive index value ~ 1.34 for rat plasma, extrapolated from previously-reported n ~ 1.35 at 630 nm for human blood plasma [34, 35]. The measured decorrelation times of CeO_2 and scattering coefficients are given in Table 4.

(II) Phantom with Au

i) The first part of this set was water phantoms with 39.95 nm diameter CeO_2 with its six different concentrations 0.1, 0.12, 0.14, 0.16, 0.18, 2.0 (weight/volume i.e. spheres/micron^3). The refractive index of Au ~ 0.47 [31], and then μ_s was calculated from Mie theory at 1310 nm [32, 33]. The refractive index of water used was 1.33. The measured decorrelation times of Au, and scattering coefficients are given in Table 4.

ii) The second part of this set was blood plasma instead of water with 39.95 nm diameter Au with its six different concentrations 0.1, 0.12, 0.14, 0.16, 0.18, 2.0 (weight/volume i.e. spheres/micron^3). Whole blood was drawn from five months old female Fisher rats into heparin tubes, which were then centrifuged to separate out the plasma. The refractive index of Au ~ 0.47 [31], and then μ_s was calculated from Mie theory at 1310 nm given in table 4 [32, 33]. Refractive index value ~ 1.34 for rat plasma, extrapolated from previously-reported n ~ 1.35 at 630 nm for human blood plasma [34, 35]. The measured decorrelation times of Au and scattering coefficients are given in table 4.

Fig. 5 represents the concentration of nanoparticles versus relaxation time and scattering coefficient. The Au has been observed to have higher decorrelation time and scattering coefficient in both water and blood plasma phantom as compared to CeO_2.

4.2. Au and CeO_2 as contrast agent

We have analyzed the gold and CeO_2 NPs using OCT system in order to observe their performance as contrast agents. The NPs as contrast agents were analyzed in deionized water and blood plasmas phantom, the obtained images are shown in Fig. 6.

Fig. 6 shows the characteristic OCT image of corresponding NPs, which are Au NPs around 39 nm and CeO_2 around 29 nm, one of the most important characteristics of this particles is the strong absorption at 1310 nm, while the scattering effect is very weak at this size as shown in Fig. 5 (b). From these images we can see just the noisy background of water and blood plasma, small CeO_2 NPs has a weak scattering, and they not permit

to show good contrast in water neither in blood plasma while the AU having relatively high scattering, shows good contrast. All images were scanned around at 3 mm depth [36, 37]. The depth profile for Au in blood plasma is shown in figure 7 for illustration purpose. The signal from the cover slip and first layer of the particles can be easily observed.

Table 4. Summary of the OCT experimental results and analysis for the two phantom sets, demonstrating the variations in concentration of scattering particles, translational decorrelation times and Scattering coefficient

Concentration of nano particles (spheres/micron^3)	**Translational decorrelation time (msec)**	**Scattering coefficient (mm^{-1})**
Phantom set (1)-Water @ CeO_2		
0.10	6.97 ± 0.25	1.749e-06
0.12	7.85 ± 0.26	2.100e-06
0.14	8.61 ± 0.28	2.450e-06
0.16	9.20 ± 0.29	2.800e-06
0.18	10.20 ± 0.29	3.150e-06
0.20	12.10 ± 0.28	4.341e-06
Phantom set (1) - Blood Plasma @ CeO_2		
0.10	7.67 ± 0.24	1.748e-06
0.12	8.15 ± 0.25	2.098e-06
0.14	9.61 ± 0.24	2.447e-06
0.16	9.96 ± 0.27	2.797e-06
0.18	11.60 ± 0.29	3.146e-06
0.20	13.60 ± 0.25	4.356e-06
Phantom set (2)- Water @ Au		
0.10	10.46 ± 0.19	1.4693e-05
0.12	11.27 ± 0.16	1.7632e-05
0.14	14.70 ± 0.18	2.0571e-05
0.16	17.12 ± 0.21	2.3510e-05
0.18	20.40 ± 0.26	2.6448e-05
0.20	24.10 ± 0.29	2.9387e-05
Phantom set (2)- Blood Plasma @ Au		
0.10	11.20 ± 0.25	1.5227e-05
0.12	12.52 ± 0.28	1.8272e-05
0.14	14.00 ± 0.25	2.1318e-05
0.16	15.90 ± 0.23	2.4363e-05
0.18	17.00 ± 0.24	2.7408e-05
0.20	20.00 ± 0.28	3.0454e-05

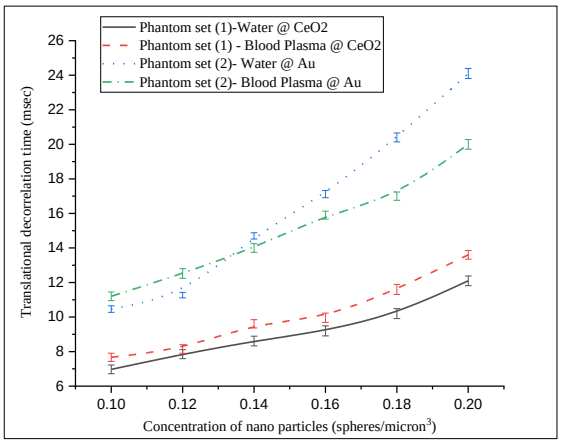

(a)

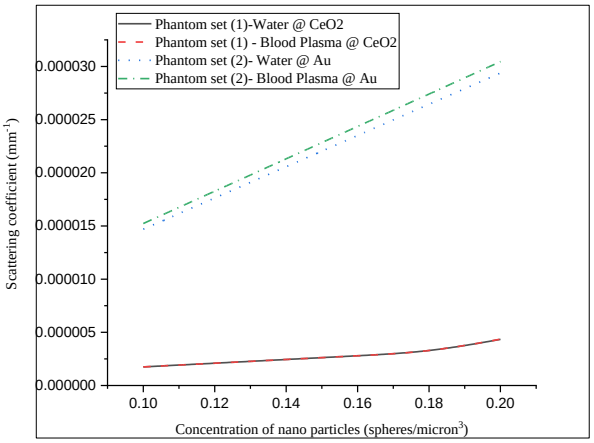

(b)

Fig. 5. Concentration of Au and CeO_2 particles as a function of (a) translational decorrelation time and (b) scattering coefficient. Au shows the higher relaxation time and scattering coefficient as compared to CeO_2 (color online)

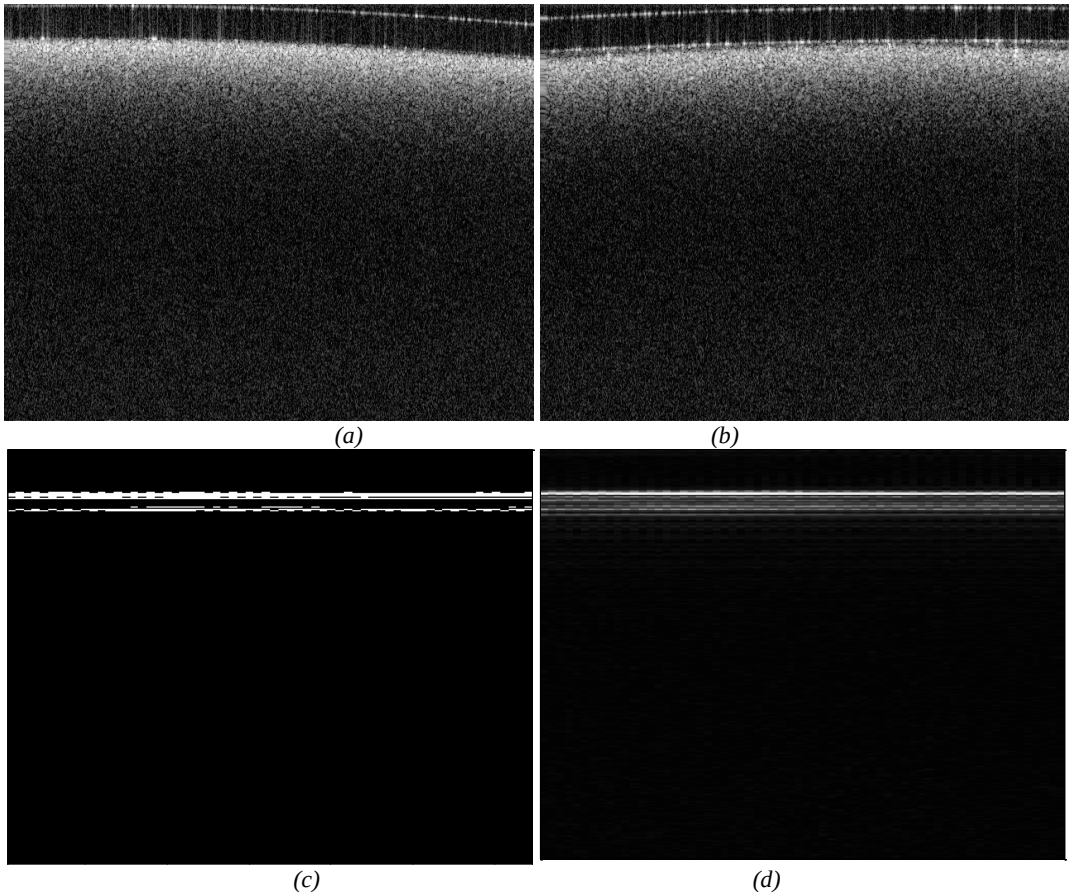

Fig. 6. OCT Images of seed (a) Au in water solution, (b) Au in blood plasma, (c) CeO_2 in water solution, and (d) CeO_2 in blood plasma phantom (color online)

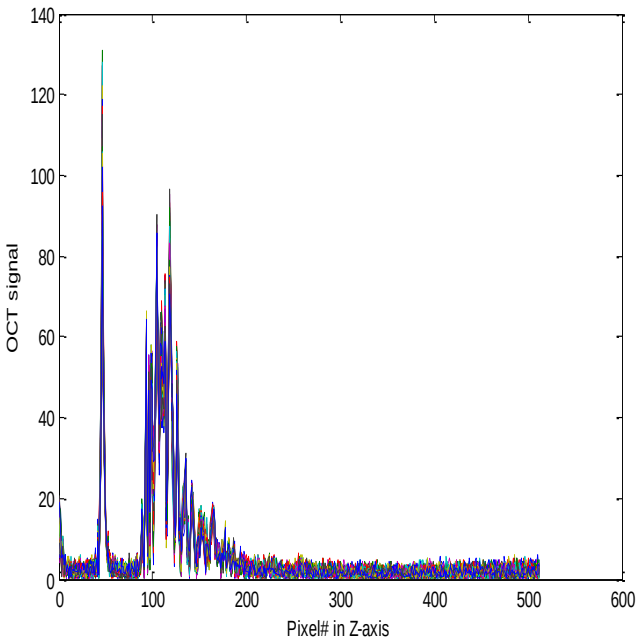

Fig. 7. The depth profile of OCT signal from Au in blood plasma for illustration purpose (color online)

5. Conclusion

In the current work, we conclude the successful synthesis and the confirmation of CeO_2/Au core shell by characterizing with UV-Vis spectroscopy and DRS. K-edge value of cerium has been found to be 40.410 KeV. These nanoparticles can be used in OCT for Brownian motion applications under dynamic light scattering and contrast agents. Gold nanoparticles have greater absorbance for x-ray because of higher atomic number and hence have biocompatibility but toxic nanoparticles. By adding thioglycolic acid as linker and starch as the targeting agent the chance of cytotoxicity is reduced and enhances the accuracy in targeting in tumour. In such a way, CeO_2/Au core shell NPs can effectively serve as the targeted OCT contrast agent.

Funding

The authors extend their appreciation to the Researchers supporting project number (RSP2024R224) King Saud University, Riyadh, Saudi Arabia.

Ethical approval

This research was conducted under the Institutional Bioethics Committee at the Islamia University of Bahawalpur, Bahawalpur, Pakistan.

References

[1] S. Das, J. M. Dowding, K. E. Klump, J. F. McGinnis, W. Self, S. Seal, Nanomedicine **8**(9), 1483 (2013).
[2] M.-C. Daniel, D. Astruc, Chemical Reviews **104**(1), 293 (2004).
[3] Seyed Enayatollah Taghavi Moghaddam, F. Emami, J. Optoelectron. Adv. Mat. **25**(3-4), 121 (2023).
[4] C. Peng, K. Li, X. Cao, T. Xiao, W. Hou, L. Zheng, R. Guo, M. Shen, G. Zhang, X. Shi, Nanoscale **4**(21), 6768 (2012).
[5] H. Wang, L. Zheng, R. Guo, C. Peng, M. Shen, X. Shi, G. Zhang, Nanoscale Research Letters **7**(1), 190 (2012).
[6] Y. Liu, Multifunctional Nanoprobes, Springer, 105 (2018).
[7] Z. Liu, Z. Li, J. Liu, S. Gu, Q. Yuan, J. Ren, X. Qu, Biomaterials **33**(28), 6748 (2012).
[8] M. Petrus, E. M. Carstea, D. C. A. Dutu, D. C. Dumitras, J. Optoelectron. Adv. M **13**(7), 776 (2011).
[9] D. Savastru, S. Miclos, N. Iftimia, M. A. Calin, R. Savastru, D. Manea, S. Dontu, J. Optoelectron. Adv. M. **18**(11-12), 993 (2016).
[10] D. Mubarak Ali, N. Thajuddin, K. Jeganathan, M. Gunasekaran, Colloids and Surfaces B: Biointerfaces **85**(2), 360 (2011).
[11] H. Huang, X. Yang, Carbohydrate Research **339**(15), 2627 (2004).
[12] D. Schubert, R. Dargusch, J. Raitano, S.-W. Chan, Biochemical and Biophysical Research Communications **342**(1), 86 (2006).
[13] F. Zhu, G. Chen, S. Sun, X. Sun, Journal of Materials Chemistry A **1**(2), 288 (2013).
[14] R. Lathe, M. Kieny, S. Skory, J. Lecocq, DNA **3**(2), 173 (1984).
[15] Z. Cheng, A. Al Zaki, J. Z. Hui, V. R. Muzykantov, A. Tsourkas, Science **338**(6109), 903 (2012).
[16] S. Munir, A. Rasheed, S. Zulfiqar, M. Aadil, P. O. Agboola, I. Shakir, M. F. Warsi, Ceramics International **46**(18, Part A), 29182 (2020).
[17] D. M. D. M.Prabaharan, K. Sadaiyandi, M. Mahendran, S. Sagadevan, Materials Research **19**(2), 478 (2016).
[18] M. H. Majles Ara, Z. Dehghani, R. Sahraei, A. Daneshfar, Z. Javadi, F. Divsar, Journal of Quantitative Spectroscopy and Radiative Transfer **113**(5), 366 (2012).
[19] S. Aswathy Aromal, K. V. Dinesh Babu, D. Philip, Spectrochimica Acta Part A: Molecular and Biomolecular Spectroscopy **96**, 1025 (2012).
[20] C.-M. Fan, L.-F. Zhang, S.-S. Wang, D.-H. Wang, L.-Q. Lu, A.-W. Xu, Nanoscale **4**(21), 6835 (2012).
[21] Hafeez Ullah, Asad Rehman Khan, Zahida Batool, Aalia Nazir, R. Khawar, Lasers in Engineering **49**(4-6), 307 (2021).
[22] J. Calvache-Muñoz, F. A. Prado, J. E. Rodríguez-Páez, Colloids and Surfaces A: Physicochemical and Engineering Aspects **529**, 146 (2017).
[23] V. Amendola, M. Meneghetti, Journal of Physical Chemistry C **113**(11), 4277 (2009).
[24] Hafeez Ullah, Ejaz Ahamd Khera, M. Malik, Lasers in Engineering **43**(4-6), 383 (2019).
[25] Kamuran Kara, Ebru Şenadim Tüzemen, R. Esen, Turkish Journal of Physics **38**(2) (2014), 238 (2014).
[26] N. Shehata, K. Meehan, M. Hudait, N. Jain, S. Gaballah, Journal of Nanomaterials **2014**, 401498 (2014).
[27] O. S. Zhernovaya, V. V. Tuchin, I. V. Meglinski, Laser Physics Letters **5**(6), 460 (2008).
[28] V. Lychagov, A. Kalyanov, V. Ryabukho, Optics and Spectroscopy **107**(6), 859 (2009).
[29] B. Veksler, E. Kobzev, M. Bonesi, I. Meglinski, Laser Physics Letters **5**(3), 236 (2008).
[30] M. Atif, H. Ullah, M. Y. Hamza, M. Ikram, Laser Physics Letters **8**(9), 629 (2011).
[31] F. Zhu, G. Chen, S. Sun, X. Sun, Journal of Materials Chemistry A **1**(2), 288 (2013).
[32] S. Prahl, Mie Scattering Calculator. http://omlc.ogi.edu/calc/mie_calc.html (2022).
[33] H. Ullah, M. Atif, S. Firdous, M. S. Mehmood, M. Ikram, C. Kurachi, C. Grecco, G. Nicolodelli, V. S. Bagnato, Laser Physics Letters **7**(12), 889 (2010).
[34] Z. Y. Guo, H. J. Guo, H. Q. Wei, Y. H.Yang, S. S. He, G. Y. Xie, H. Q. Wu, Zhong, L. Q. Li, Q. L. Zhao, Laser Phys. **20**, 1849 (2010).
[35] J. Y. Jin, L. Chen, L. Xu, P. N. Wang, Physics in Medicine and Biology **51**(20), N371 (2006).
[36] Y. Ponce de León, J. L. Pichardo-Molina, N. Alcalá Ochoa, D. Luna-Moreno, Journal of Nanomaterials **2012**, 571015 (2012).
[37] Y. R. Ponce-de-Leon, J. A. Lopez-Rios, J. L. Pichardo-Molina, and N. Alcalá Ochoa, Proc. SPIE 8011, 22nd Congress of the International Commission for Optics: Light for the Development of the World, 80118W (2011).

*Corresponding author: hafeezullah@iub.edu.pk